

## Late-Time Coarsening Dynamics in a Nematic Liquid Crystal

Isaac Chuang,<sup>(1)</sup> Neil Turok,<sup>(2)</sup> and Bernard Yurke<sup>(1)</sup>

<sup>(1)</sup>*AT&T Bell Laboratories, Murray Hill, New Jersey 07974*

<sup>(2)</sup>*Joseph Henry Laboratories, Princeton University, Princeton, New Jersey 08544*

(Received 8 November 1990)

We have studied the coarsening dynamics of line defects in the uniaxial nematic liquid crystal 4-cyano-4'-n-pentylbiphenyl, subjected to a rapid pressure jump from the isotropic to the nematic phase. At late times, the density of disclination lines  $\rho$  is expected to scale with time as  $\rho \propto t^{-\nu}$  with  $\nu=1$ . We have measured the scaling exponent to be  $\nu=1.02 \pm 0.09$  over the region  $16 < \rho < 160 \text{ mm}^{-2}$ . In addition, we have measured the collapse of loops consisting of type- $\frac{1}{2}$  disclination lines. The loop radius  $r$  is expected to scale with time as  $r \propto (t_0 - t)^\alpha$ , where  $\alpha = \frac{1}{2}$  and  $t_0$  is the time at which the loop vanishes. We found  $\alpha$  to be  $0.50 \pm 0.03$ .

PACS numbers: 64.60.Cn, 05.70.Fh, 61.30.Jf

The ordering dynamics of a physical system that has undergone a deep quench from a phase of higher symmetry to a phase of lower symmetry is a topic of considerable interest.<sup>1-5</sup> The behavior of such systems is expected to depend on the dimensionality and internal symmetry of the system, and the presence of conservation laws. The bulk of the experimental and theoretical work that has been reported is on the phase-separation dynamics (spinodal decomposition) of binary mixtures. More recently, attention has also focused on systems whose Hamiltonian has a continuous<sup>6-11</sup> rather than discrete symmetry. Generally, theoretical work has concentrated on models characterized by the time-dependent Landau-Ginzburg equation.<sup>9</sup> For such models, with nonconserved order parameter, it is generally predicted<sup>7,11</sup> that the defect line density should scale as  $t^{-1}$ . However, a scaling behavior of  $t^{-0.75 \pm 0.05}$  from numerical simulations has been reported for line defects in three dimensions,<sup>9</sup> and  $t^{-1.00 \pm 0.04}$  for vortex defects in two dimensions.<sup>6</sup> The coarsening dynamics of systems undergoing phase transitions by breaking a continuous symmetry are also of considerable interest in cosmology. In particular, models employing such phase transitions have been proposed to account for the large-scale structure of the Universe.<sup>12-15</sup>

Although there has been considerable theoretical and numerical work on the coarsening dynamics of systems with a continuous symmetry there appears to be little experimental work. Orihara, Ishibashi, and Nagaya have studied<sup>16,17</sup> two-dimensional coarsening dynamics in thin films of uniaxial nematic liquid crystal subjected to rapid thermal quenches and measured a scaling of  $t^{0.44}$  for the correlation length. For this system coarsening proceeds primarily by the collapse of disclination loops and the line density is expected to scale as  $t^{-1/2}$ . In this Letter, we report experimental studies of the three-dimensional coarsening dynamics of a uniaxial nematic liquid crystal subjected to a rapid, pressure-jump-initiated isotropic to nematic phase transition. The disclination line density for this system is expected to scale as  $t^{-1}$ . We have also

studied loop collapse to verify the dynamics on which the scaling prediction is based.

The order parameter<sup>18,19</sup> for the liquid crystal is described by a second-rank traceless symmetric tensor. The phase transition from the isotropic phase (the high-temperature or low-pressure phase) to the nematic phase (the low-temperature or high-pressure phase) thus involves breaking from a SO(3) to an O(2) symmetry.<sup>20-22</sup> The vacuum manifold  $\mathcal{M}_0$  for the nematic phase is the projective two-sphere  $\mathcal{S}_2/\mathcal{Z}_2$ . Singular defects found in the nematic phase include type- $\frac{1}{2}$  disclination lines belonging to the  $\pi_1(\mathcal{M}_0)$  homotopy class, and singly charged monopoles belonging to the  $\pi_2(\mathcal{M}_0)$  homotopy class. The nematic liquid crystal can also support texture, belonging to the  $\pi_3(\mathcal{M}_0)$  homotopy class, although these nonsingular objects appear to be very rare. Also found in the uniaxial nematic phase are type-1 disclination lines. In a companion paper,<sup>23</sup> we discuss the dynamics of these defects in more detail. Upon a rapid pressure quench from the isotropic phase to the nematic phase, a dense tangle of these defects is formed through the Kibble mechanism.<sup>24</sup> This tangle evolves to decrease the system's energy. At late times, the dynamics of the tangle are dominated by type- $(\pm \frac{1}{2})$  and type-1 disclination lines. The type- $\frac{1}{2}$  disclination lines are more energetic than the type-1 disclination lines, and hence determine the late-time dynamics.

The dynamics of the disclination lines are controlled by the string tension and the viscous forces. In particular, the line tension  $T$  scales as  $\ln R/r_c$ , where  $r_c$  is the core radius and  $R$  is the typical spacing between disclination lines. For a disclination line moving through the medium with a constant velocity  $v$ , one can show, using nematodynamic equations,<sup>18</sup>

$$\gamma \partial_t \mathbf{n} = - \frac{\delta \mathcal{E}}{\delta \mathbf{n}}, \quad (1)$$

that the damping force  $\Gamma$  is also proportional to  $\ln R/r_c$ .  $\mathcal{E}$  is the Frank free energy.<sup>18,19</sup> The ratio  $T/\Gamma$  should

thus be independent of  $R$ . We have tested this expectation by measuring the rate of collapse of disclination loops. In particular, for a loop of radius  $r$ , one has  $-\Gamma dr/dt = T/r$ , which when integrated yields

$$r = [(2T/\Gamma)(t_0 - t)]^{1/2}. \quad (2)$$

One thus expects the loop radii to shrink with time via  $r \propto (t_0 - t)^\alpha$ , with  $\alpha = 0.5$ .

This simple model for disclination-line dynamics allows for an argument (of the Lifshitz-Slyosov type<sup>25</sup>) about how the late-time coarsening dynamics should proceed provided that one postulates that the string network should be characterized by a single scale  $\xi$ , defined by  $\rho \equiv \xi^{-2}$ , where  $\rho$  is the line length per unit volume. The typical radius of curvature of the strings and the typical interstring separation are both proportional to  $\xi$ .

The characteristic velocity  $v$  of a string is found by equating the characteristic line tension force, which is proportional to  $T/\xi$ , with the characteristic friction force  $\Gamma v$  per unit length. One finds  $v \propto T/\Gamma\xi$ . The rate of loss of energy from the string network is thus  $W = Tvp/\xi = T^2\rho^2/\Gamma$  per unit volume. The rate of decrease of  $\rho$  can be calculated by equating this energy loss with the time derivative of the string energy density  $W \propto T\rho$  to get

$$\frac{d\rho}{dt} = -c \frac{T}{\Gamma} \rho^2, \quad (3)$$

where a constant of proportionality,  $c$ , has been introduced.

Second, we should include the loss of length from the long strings into loops: This is always favored by phase space over reconnection of loops onto a long string.<sup>26</sup> A long string loses length to loops at a rate given by a geometrical constant times  $v/\xi$ , which scales the same way as the viscous-force damping term. Thus, the constant  $c$  may be taken to include both these effects. Integrating Eq. (3), we find that the scaling solution is given by  $\rho = (\Gamma/cT)t^{-\nu}$ , with  $\nu = 1$ .

We experimentally tested the  $\rho \propto t^{-1}$  string-density scaling prediction and the  $r \propto (t_0 - t)^{0.5}$  loop-collapse rate equation by recording high-speed video pictures of the string network which formed after performing a rapid pressure jump (of  $\Delta P$ ) to force an isotropic to nematic phase transition. The data were analyzed using simple image-processing techniques.

We studied the nematic liquid crystal 4-cyano-4'-n-pentylbiphenyl,<sup>27,28</sup> also referred to as K15 or CB5. The material we used was obtained from BDH Chemicals, and used without further purification. At atmospheric pressure the isotropic to nematic phase transition occurs at 35.3°C. We measured the slope  $\Delta P/\Delta T$  of the coexistence curve to be 2.47 MPa/K, between 0.7 and 17 MPa.

Our apparatus consisted of a pressure cell and supporting pressurization and data-acquisition hardware. The cell contained the liquid crystal between two sap-

phire observation windows, and was isolated from the pressurization fluid by a Kapton diaphragm connected via a short segment of high-pressure tubing. A thermocouple and heating wire were attached to the pressure chamber to provide temperature control, and the whole cell was encased in Styrofoam to provide insulation. Pressure jumps were initiated by opening a valve connecting the diaphragm to a hand-turned piston containing water. The sapphire windows were treated with homeotropic alignment material, *N,N*-dimethyl-*N*-octadecyl-3-aminopropyltrimethoxysilyl chloride (DMOAP), using standard procedures.<sup>29</sup>

The cell was mounted on a transmission observation microscope, and a high-speed video camera with a 5-ms resolution clock was used to record data onto videotape. We estimated that the phase transition occurred in less than 30 ms. A switch mounted on the jump valve was found to give a good reading for  $t = 0$ . Defect-tangle-evolution observations were replayed from the tapes and digitized for computer analysis. Simple image-processing schemes were used to enhance the images and to estimate the string density. We measured the depth of the cells to be  $158 \pm 8 \mu\text{m}$  for the  $\Delta P = 2.00$  MPa run and  $234 \pm 23 \mu\text{m}$  for the other three. All the data were taken using a 10× objective, with a depth of field large enough such that all defects anywhere between both surfaces of the windows were clearly identifiable. With greater cell thicknesses, we found that identifying strings became more difficult, because of occlusions and light scattering.

Coarsening data were taken for pressure jumps of  $\Delta P = 2.00, 2.28, 2.62,$  and  $4.69$  MPa, from an initial state in the isotropic phase with  $T = 33 \pm 1^\circ\text{C}$  and  $P = 3.6$  MPa. Data from ten jumps for each  $\Delta P$  were recorded, and then pictures of the string tangle at various times were digitized to be analyzed by the computer. Four typical pictures of the string tangle in evolution are shown in Fig. 1. Loop-collapse data were taken from the same data, by selecting runs which happened to leave nearly circular isolated loops at a late stage in the evolution of the system.

The guiding principle behind our application of image processing to clarify the string-tangle pictures was to do as little processing as possible before estimating the string density. We used a four-step analysis, including  $3 \times 3$  median filtering, adaptive background subtraction, Sobel gradient calculation, and a cleaning algorithm similar to morphological dilation and erosion.<sup>30</sup> Adaptive background subtraction was accomplished by dividing the  $512 \times 400$  images into  $128 \times 100$ -sized subimages, calculating for each region the average of each of the  $32 \times 25$  subregions weighted by its standard deviation, fitting a *B* spline to the subimage points to get  $512 \times 400$  "background" images, and subtracting these from the original images. The grey levels were then rescaled such that the mean was a light grey and the standard devia-

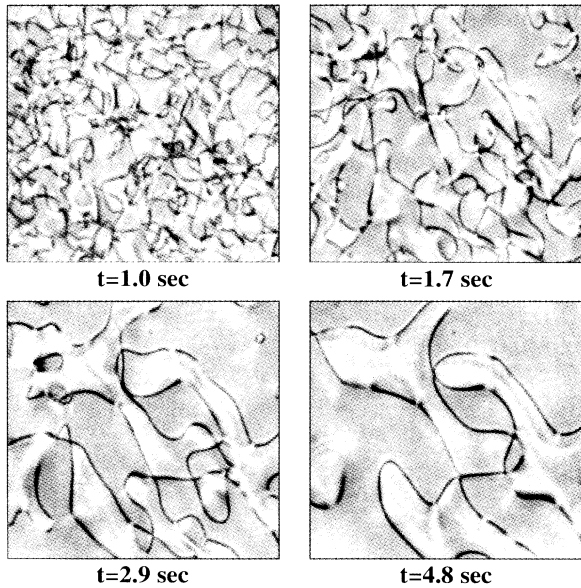


FIG. 1. A coarsening sequence showing the strings visible in our 230- $\mu\text{m}$ -thick pressure cell containing K15 nematic liquid crystal, at  $t=1.0, 1.7, 2.9,$  and  $4.8$  s after a pressure jump of  $\Delta P=4.7$  MPa from an initially isotropic state in equilibrium at approximately  $33^\circ\text{C}$  and  $3.6$  MPa. The evolution of the string network shows self-similar or “scaling” behavior. Each picture is about  $360\ \mu\text{m}$  wide.

tion spanned the resolution of the display. This successfully normalized the light intensity across our images. Finally, the string density was estimated from the processed images by counting the number of points above a set threshold. We chose to calibrate the string density so that it represents the number of strings per unit area crossing a plane. The calibration for each data set was obtained by counting the number of strings crossing a line drawn across the image, averaged over several lines and images, and dividing by the cross-sectional area, i.e., the depth of the cell times the width of the image.

We found that for times between 1 and 32 s, the string network was low enough in density for the strings to be clearly distinguished. Our string-density results are shown in Fig. 2. The statistical errors, obtained by averaging over several runs, are smaller than the symbol sizes. Repeating the experiment at increasing  $\Delta P$ , we found the same scaling with time, but decreasing string density at a fixed time, consistent with the effect expected, where if the string tension is increased, so is the scaling value of  $\xi$ .

The data do show systematic deviations from straight-line behavior. We expect that at early times line thickness (caused by the finite camera resolution) spuriously lowers the calculated string density because of string overlap, and that, at late times, image noise significantly increases the density estimation (it is not as detrimental to the early-time data, because the amount

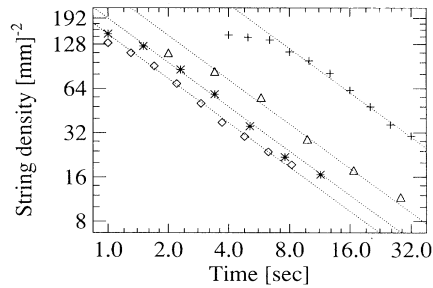


FIG. 2. String-density data, accumulated at four different  $\Delta P$ . Plus symbols correspond to  $\Delta P=2.00$ , triangles to  $\Delta P=2.28$ , asterisks to  $\Delta P=2.62$ , and diamonds to  $\Delta P=4.69$ . The dashed lines have slope  $-1$ . The scaling relationship was experimentally determined to be  $\xi \approx t^{0.51 \pm 0.02}$ , where  $\rho \equiv 1/\xi^2$ . For greater  $\Delta P$ , the string tension is higher and one expects from the analysis in the text for the scaling density to be lower, as is observed.

of noise is constant, and the string density is higher for smaller  $t$ ). Omitting the first and last points in each data set, a least-squares fit gives a scaling exponent of  $\nu=1.02 \pm 0.04$ , which is close to the predicted  $t^{-1}$  power law.

Interpretation of the data is, however, complicated by possible finite-size effects due to the interaction defects with the window surfaces. We saw no evidence of pinning of defects to the windows. Consequently, it may have been possible for the defect tangle to pull away from the windows and become concentrated in the center of the cell. To check this possibility, we studied the evolution of the number of string crossings. The vertex density should scale with the string density, as  $\rho_v \propto \rho^2$ . Figure 3 shows our results from analyzing data from the  $\Delta P=4.69$  MPa run. The data points at late times show a consistent deviation below the  $t^{-2}$  behavior expected for a three-dimensional system whose line density is given to scale as  $t^{-1}$ . However, at early times there is good agreement.

A model for the deviation observed in the behavior of

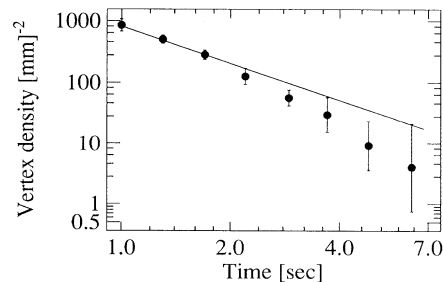


FIG. 3. The vertex density as a function of time for the  $\Delta P=4.69$  run. The error bars indicate the statistical errors, by averaging eight data sets. The solid line shows the expected  $t^{-2}$  scaling for the bulk.

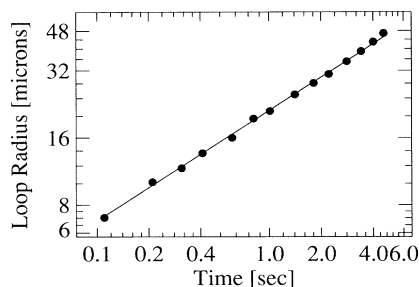


FIG. 4. Typical data showing the loop radius as a function of  $t_0 - t$ , where  $t_0$  is the time at which the loop disappears.

$\rho_c$  vs  $t$  can be constructed by assuming that the cause is a shrinking of the effective thickness  $d$  of the defect layer in the pressure cell. Thus, by extracting  $d$  from the data in Fig. 3, a correction for the proper string density  $\rho$  can be estimated. Using this procedure, and fitting to the linear regime in the corrected  $\ln \rho$  vs  $\ln t$  data, a corrected scaling exponent of  $\nu_c = 0.93 \pm 0.06$  is obtained. This number can be understood as a bound on possible deviations in bulk behavior for the coarsening exponent  $\nu$ , and is reasonably incorporated as an additional contribution to the error bars originally given for  $\nu$ . Our conclusion is that the bulk scaling exponent for our K15 system is  $\nu = 1.02 \pm 0.09$ .

To check if the disclination line dynamics used to obtain Eqs. (2) and (3) properly characterize the behavior of disclination lines, we studied the behavior of collapsing loops. Figure 4 shows data from a typical loop collapse, for which the exponent was  $\alpha = 0.49 \pm 0.002$ . Loop-collapse exponents were measured from seven events for which the loops had an eccentricity less than 0.6. The measured exponents were  $0.544 \pm 0.002$ ,  $0.494 \pm 0.002$ ,  $0.497 \pm 0.006$ ,  $0.453 \pm 0.020$ ,  $0.443 \pm 0.021$ ,  $0.520 \pm 0.005$ , and  $0.522 \pm 0.053$ . Averaging these results gives  $\alpha = 0.50 \pm 0.03$ , which is in agreement with the expected value of 0.50. We found that loops did not leave monopoles behind, nor did they collapse around monopoles. Hence, these loops must have consisted of equal numbers of  $+\frac{1}{2}$  and  $-\frac{1}{2}$  string segments. Finally, from Eq. (2), we estimated that  $T/\Gamma$  varied from about 200 to 300  $\mu\text{m}^2/\text{s}$  in the 5.6–8.3-MPa, 33°C regime.

N.T. acknowledges the support of NSF Contract No. PHY80-19754 and the Alfred P. Sloan Foundation. We wish to thank P. E. Cladis for stimulating and useful dis-

cussions.

- <sup>1</sup>H. Furukawa, *Adv. Phys.* **34**, 703 (1985).
- <sup>2</sup>P. C. Hohenberg and B. I. Halperin, *Rev. Mod. Phys.* **49**, 435 (1977).
- <sup>3</sup>P. W. Voorhees, *J. Stat. Phys.* **38**, 231 (1985).
- <sup>4</sup>J. D. Gunton, M. San Miguel, and P. S. Sahni, in *Phase Transitions and Critical Phenomena*, edited by C. Domb and J. L. Lebowitz (Academic, London, 1983), p. 267.
- <sup>5</sup>A. J. Bray, *Phys. Rev. Lett.* **62**, 2841 (1989).
- <sup>6</sup>M. Mondello and N. Goldenfeld, *Phys. Rev. A* **42**, 5865 (1990).
- <sup>7</sup>H. Toyoki and K. Honda, *Prog. Theor. Phys.* **78**, 237 (1987).
- <sup>8</sup>H. Toyoki, *Phys. Rev. A* **42**, 911 (1990).
- <sup>9</sup>H. Nishimori and T. Nukii, *J. Phys. Soc. Jpn.* **58**, 563 (1988).
- <sup>10</sup>F. de Pasquale and P. Tartaglia, *Phys. Rev. B* **33**, 2081 (1986).
- <sup>11</sup>G. F. Mazenko and M. Zannetti, *Phys. Rev. B* **32**, 4565 (1985).
- <sup>12</sup>A. Vilenkin, *Phys. Rep.* **121**, 263 (1985).
- <sup>13</sup>N. Turok, *Phys. Rev. Lett.* **63**, 2625 (1989).
- <sup>14</sup>C. T. Hill, D. N. Schramm, and J. N. Fry, *Comments Nucl. Part. Phys.* **19**, 25 (1989).
- <sup>15</sup>W. H. Press, B. S. Ryden, and D. N. Spergel, *Astrophys. J.* **347**, 590 (1989).
- <sup>16</sup>H. Orihara, *J. Phys. Soc. Jpn.* **55**, 2151 (1986).
- <sup>17</sup>T. Nagaya, H. Orihara, and Y. Ishibashi, *J. Phys. Soc. Jpn.* **56**, 3086 (1987).
- <sup>18</sup>P. G. de Gennes, *The Physics of Liquid Crystals* (Clarendon, Oxford, 1974).
- <sup>19</sup>G. Vertogen and W. H. de Jeu, *Thermotropic Liquid Crystals* (Springer-Verlag, Berlin, 1988).
- <sup>20</sup>N. D. Mermin, *Rev. Mod. Phys.* **51**, 591 (1979).
- <sup>21</sup>Louis Michel, *Rev. Mod. Phys.* **52**, 617 (1980).
- <sup>22</sup>M. Kleman, *Points, Lines, and Walls, in Liquid Crystals, Magnetic Systems, and Various Ordered Media* (Wiley, Chichester, 1983).
- <sup>23</sup>I. L. Chuang, R. Durrer, N. Turok, and B. Yurke (to be published).
- <sup>24</sup>T. W. B. Kibble, *J. Phys. A* **9**, 1387 (1976).
- <sup>25</sup>I. M. Lifshitz and V. V. Slyosov, *J. Phys. Chem. Solids* **19**, 35 (1961).
- <sup>26</sup>A. Albrecht and N. Turok, *Phys. Rev. D* **40**, 973 (1989).
- <sup>27</sup>P. P. Karat and N. V. Madhusudana, *Mol. Cryst. Liq. Cryst.* **40**, 239–245 (1977).
- <sup>28</sup>Shin-Tson Wu and R. J. Cox, *J. Appl. Phys.* **64**, 821 (1988).
- <sup>29</sup>Frederic J. Kahn, *Appl. Phys. Lett.* **22**, 386 (1973).
- <sup>30</sup>Rafael C. Gonzalez and Paul Wintz, *Digital Image Processing* (Addison-Wesley, Menlo Park, CA, 1987).

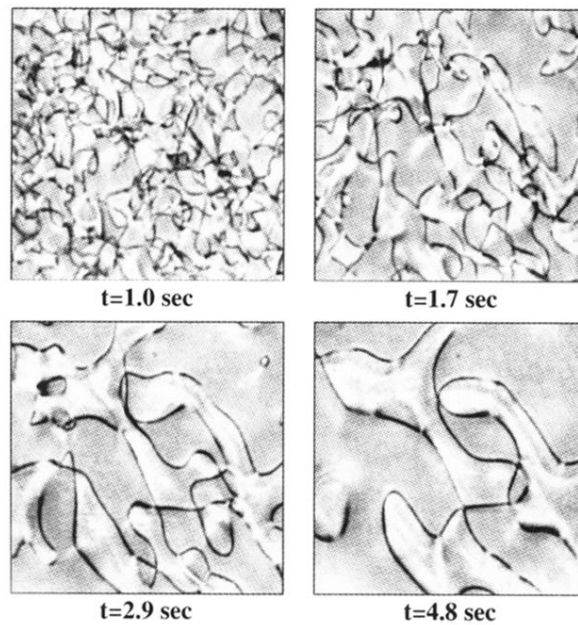


FIG. 1. A coarsening sequence showing the strings visible in our  $230\text{-}\mu\text{m}$ -thick pressure cell containing K15 nematic liquid crystal, at  $t = 1.0, 1.7, 2.9,$  and  $4.8$  s after a pressure jump of  $\Delta P = 4.7$  MPa from an initially isotropic state in equilibrium at approximately  $33^\circ\text{C}$  and  $3.6$  MPa. The evolution of the string network shows self-similar or “scaling” behavior. Each picture is about  $360\ \mu\text{m}$  wide.